

Unveiling Hydroacoustic Signatures of Aircraft Crashes: Insights from the MH370 Case

Usama Kadri

School of Mathematics, Cardiff University, UK

INTRODUCTION AND MAIN RESULTS

Aircraft impacts at sea radiate distinctive low-frequency pressure signatures detectable over thousands of kilometres; using CTBTO hydrophones, we characterise crash acoustics and revisit MH370 within narrowly defined time-bearing windows.

Ten past incidents reveal three signature types and basin-scale detectability (including land-coupled paths); for MH370, no plausible signal at H01W falls within the expected window, motivating controlled-energy tests along the 7th arc.

Background. The Argentine submarine ARA San Juan tragically imploded in November 2017 due to technical malfunctions, killing all 44 crew members on board and highlighting significant safety challenges within Argentina's naval fleet.

The submarine's explosion was recorded not only at H10 and H04 (direct water paths) **but also at H03S despite ~2,000 km of intervening land**, showing low-frequency energy coupled into the seabed (Scholte → Rayleigh) and re-entered the ocean; the H03S amplitude was only 21% of H04S and 11% of H10N due to land losses. **The shortest-time path** (~1,900 km in solid at ~3,550 m/s + ~330 km in water at ~1,480 m/s → 12-13.5 min) **matches the observed arrival and bearing** (~105.6°) at H03S, unlike bearings expected from water-only or shortest-distance paths. A **calibration grenade** dropped near the site on 1 Dec 2017 reproduced the timing (~13 min), duration (~30 s), band, and a secondary arrival 1.5 min later, corroborating the interpretation.

Kadri, U. Underwater acoustic analysis reveals unique pressure signals associated with aircraft crashes in the sea: revisiting MH370. *Sci Rep* 14, 10102 (2024)

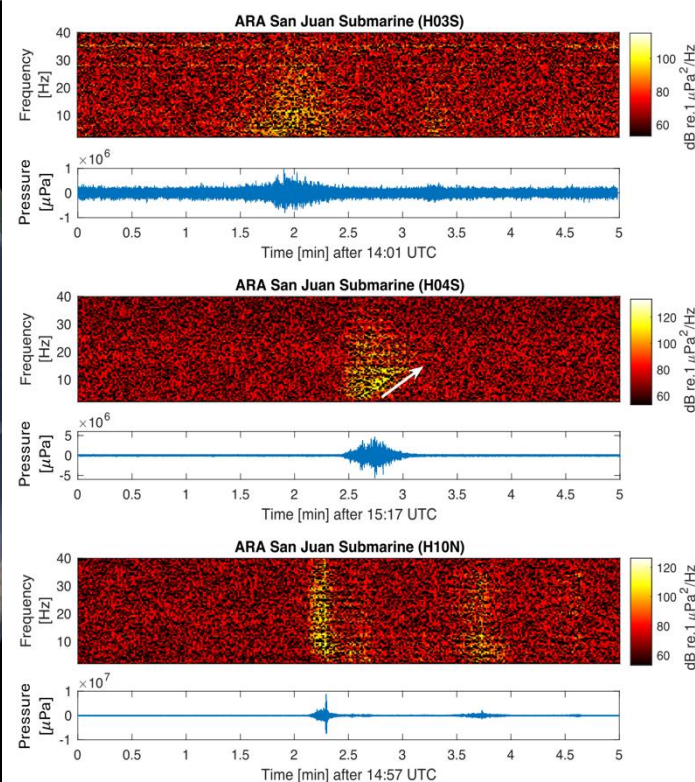
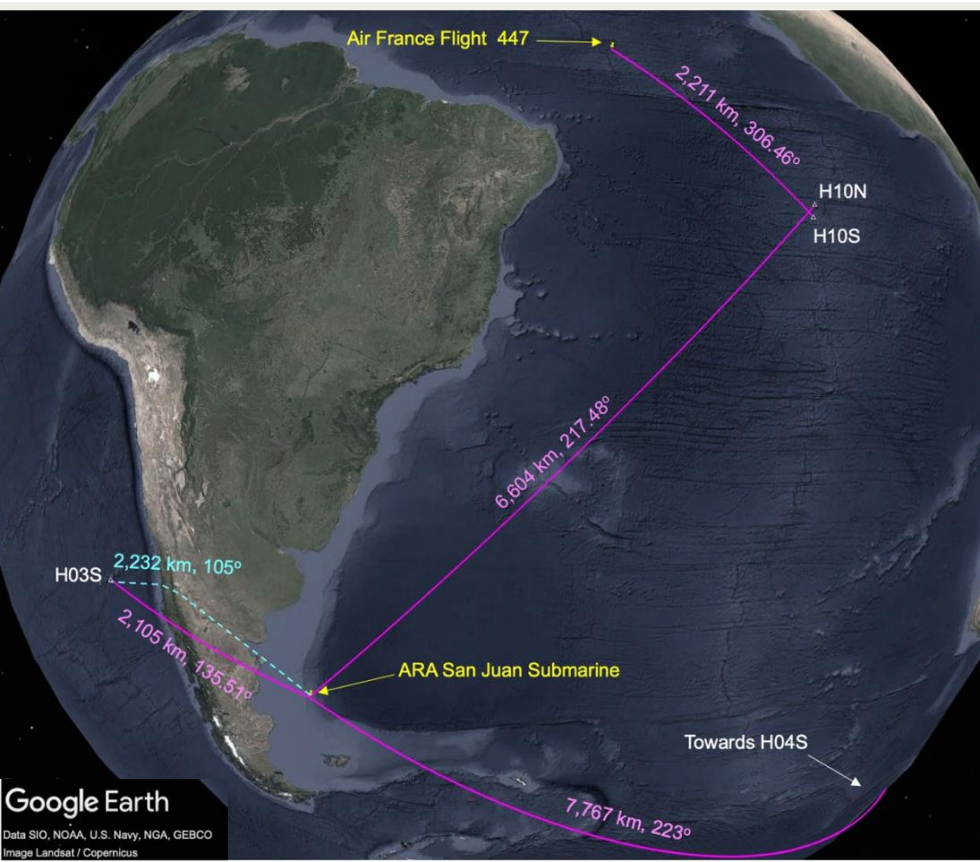


Figure 7. Spectrogram and pressure time series of ARA San Juan Submarine explosion recorded at stations H03S (top), H04S (middle), and H10N (bottom). White arrow highlights dispersion.

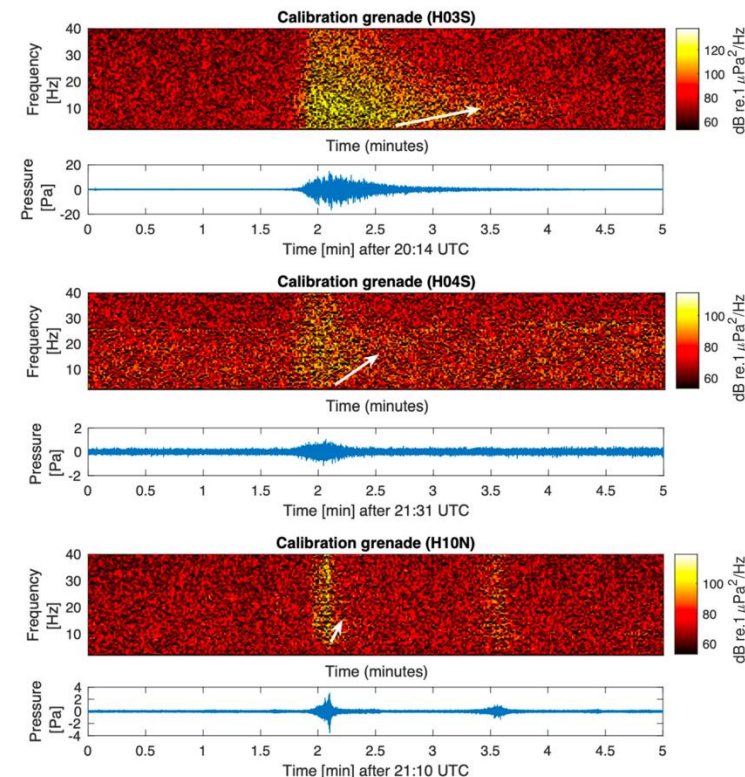
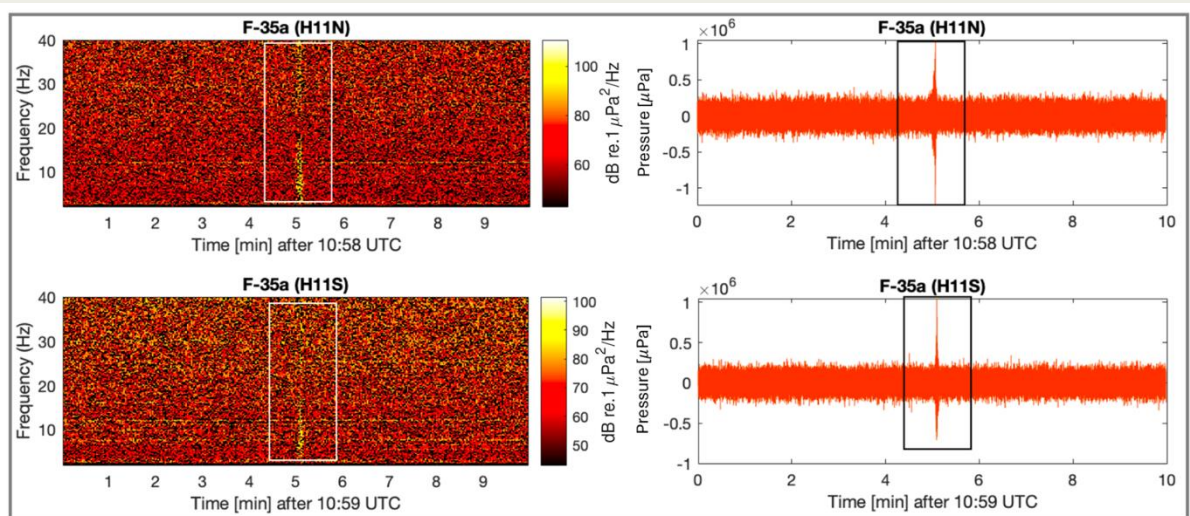
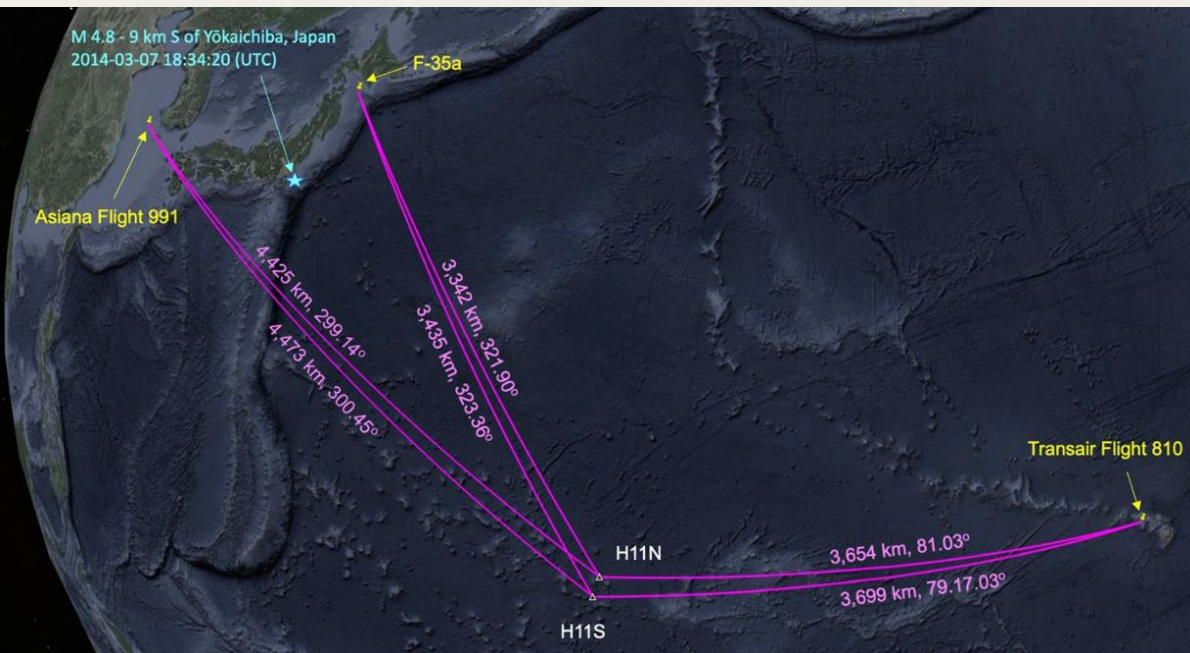


Figure 8. Spectrogram and pressure time series of a calibration grenade recorded at stations H03S (top), H04S (middle), and H10N (bottom). White arrow highlights dispersion.



Background. The Japanese F-35A fighter jet crashed into the Pacific Ocean on April 9, 2019, during a night training mission near Misawa Air Base.

Main result. A sharp, ~ 6 s broadband pulse from the supersonic impact was cleanly detected at both Wake Island arrays (H11N/H11S) over $\sim 3,300$ km away, illustrating basin-scale detectability of high-energy crashes. The propagation transect shows a clear, unobstructed water path, minimal bathymetric scattering, explaining the strong, distinct recording at both arrays.

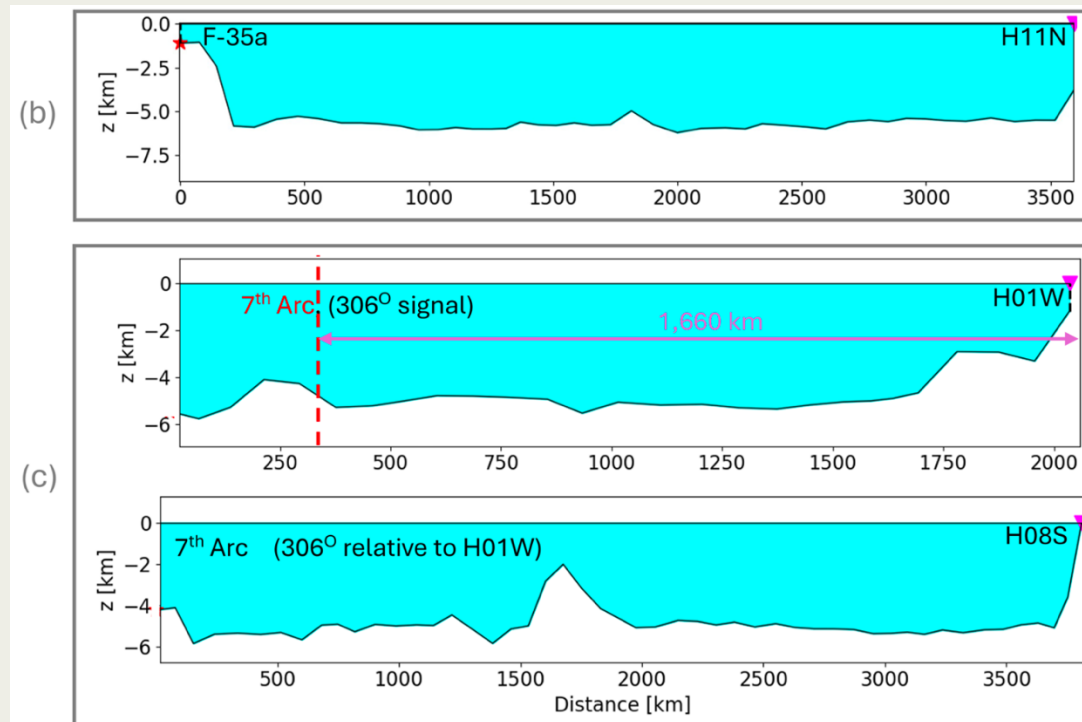


Figure 15. Transects of events to corresponding hydrophones. (a) ARA San Juan Submarine: a large barrier (Rio Grande Rise) half way to H10N; smaller barriers observed in the direction of H04S. (b) F-35a: clear path with no barriers observed. (c) Bearing 306°: clear path with a minor barrier towards the end in the direction of H01W; a large barrier half way to H08S.

Background. MH370 vanished on 8 Mar 2014 with 239 on board; official analysis constrains impact to the **Southern Indian Ocean** near the **Inmarsat 7th arc (00:19:29 UTC)**, implying a high-energy sea impact. For hydroacoustic verification, the relevant CTBTO stations are **H01W (Cape Leeuwin)** and **H08S (Diego Garcia)** at **~1600 km** and **~3700 km** from the arc, respectively.

Main result: within the narrow time-bearing window, **no candidate signal** appears at **H01W** (nor H08) despite the short path compared to F-35a case.

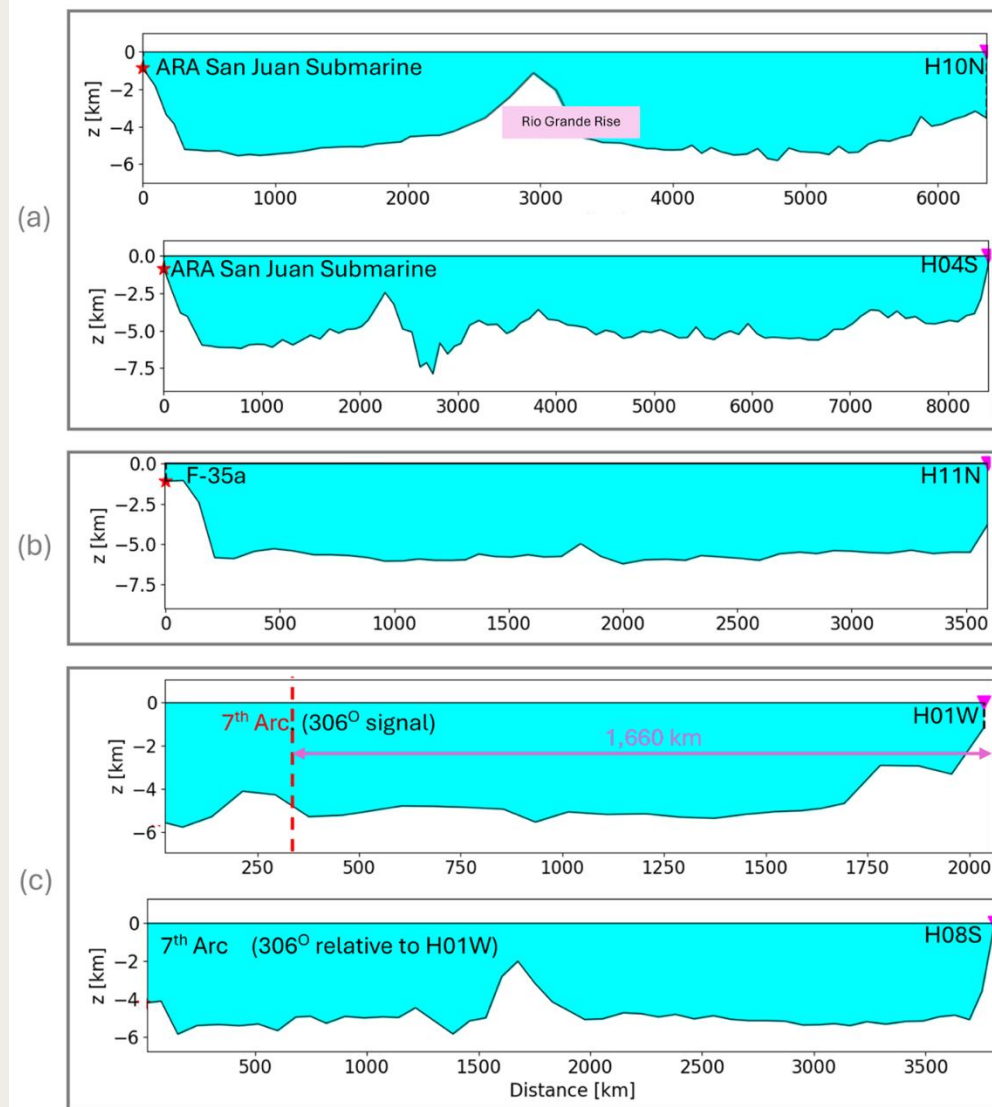
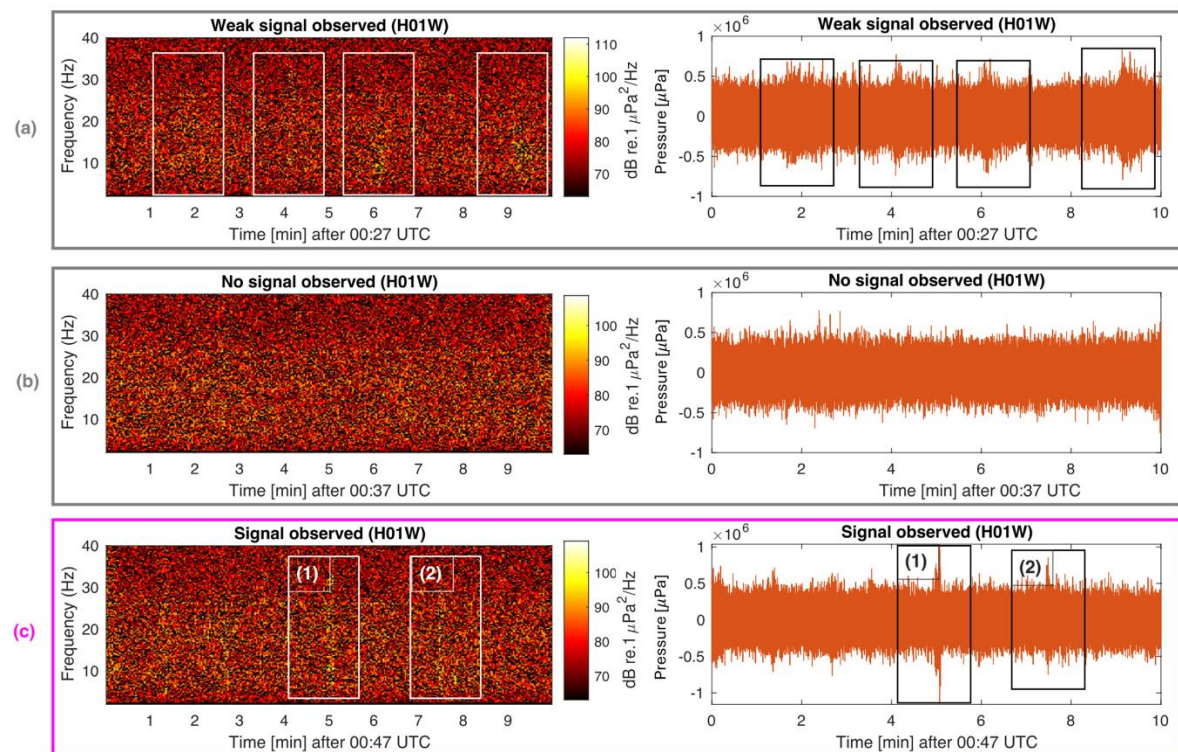


Figure 15. Transects of events to corresponding hydrophones. (a) ARA San Juan Submarine: a large barrier (Rio Grande Rise) half way to H10N; smaller barriers observed in the direction of H04S. (b) F-35a: clear path with no barriers observed. (c) Bearing 306°: clear path with a minor barrier towards the end in the direction of H01W; a large barrier half way to H08S.

Conclusions/Action

Basin-scale detectability. Crash-generated pressure signatures are observable at **thousands of kilometres**, including after land crossings, enabling classification and timing under noisy conditions.

MH370 insight (not definitive). Within official constraints, no signal at H01W fits the window; lack of H08S confirmation is consistent with noise and bathymetric loss → further evidence required.

Actionable next step. Conduct **controlled explosions / airguns** along the 7th arc (energy comparable to a high-impact crash) to calibrate amplitudes/paths and refine localisation strategy.

General framework. Entropy-guided detection, bearing, & bathymetry-aware propagation offers a reproducible workflow for **crash forensics** and related high-energy ocean events.

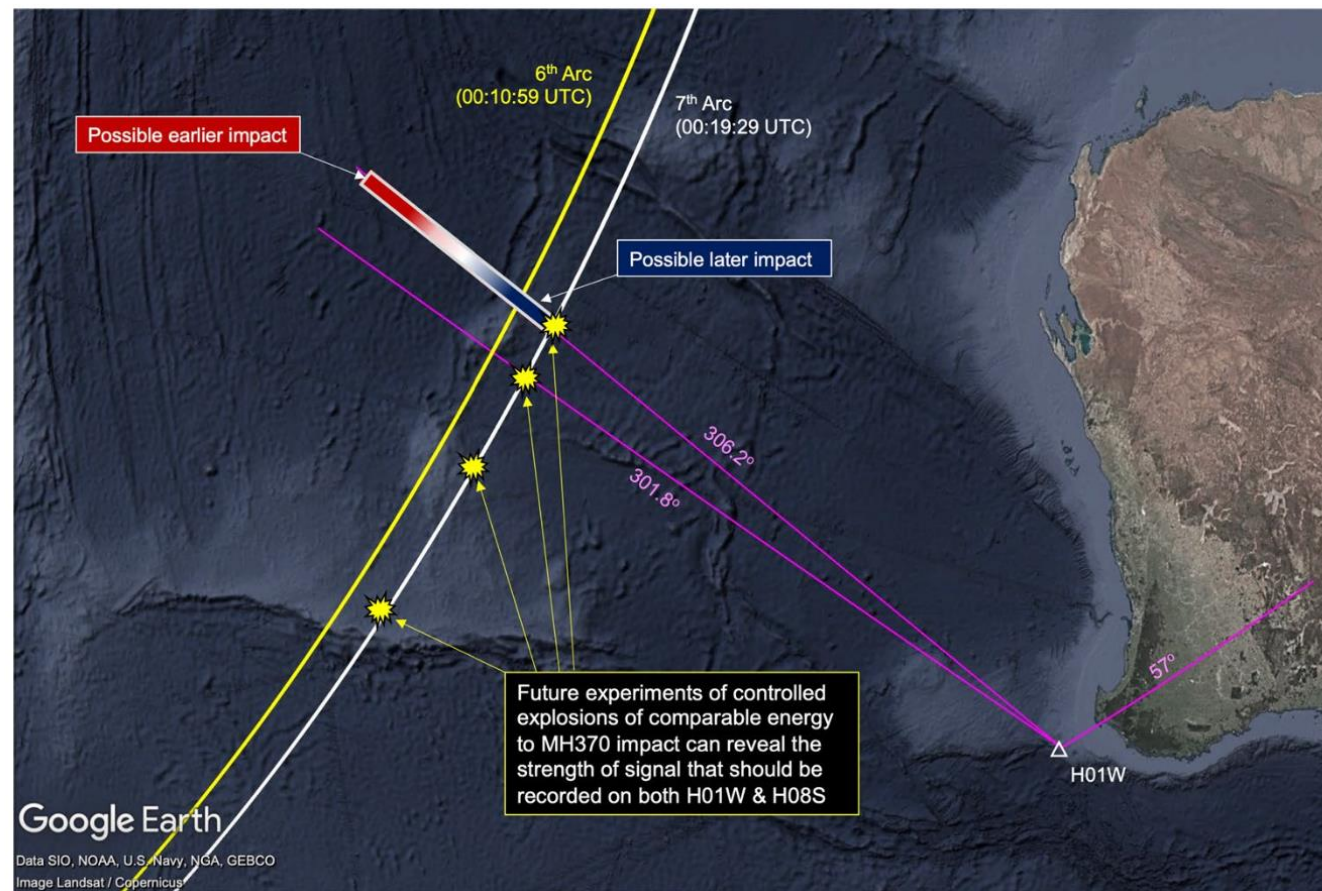


Figure 10. Location of the CTBTO's hydroacoustic station H01W (white triangle); Inmarsat 6th arc at 00:10:59 UTC (yellow curve); Inmarsat 7th arc at 00:19:29 UTC (white curve). The possible impact location of the source of signal (2) of Fig. 9c is presented in a gradient rectangle (red for earlier impact, and blue for later impact). Suggested future controlled explosions of comparable energy to MH370 are illustrated by yellow explosion symbol.

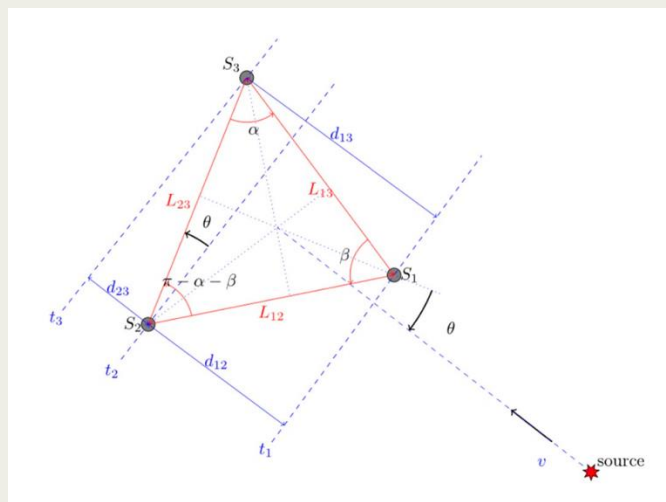
Methods/Data

Data & cases. CTBTO IMS hydroacoustic stations (H01W, H08S/N, H11N/S, etc.); ~100 h targeted around event windows; ten aircraft crashes, and submarine implosion.

Pre-processing & detection. High-pass (<5 Hz) + 2-40 Hz band-pass; windowed entropy to flag transients; TOA cross-correlation across 3-hydrophone arrays to compute bearing ($\pm 0.4^\circ$ at 99.5% CI).

Propagation analysis. Bathymetric transects to assess scattering/loss; shortest-time paths allow **water-seabed-land coupling** (Scholte/Rayleigh) explaining signals recorded after long over-land legs (ARA *San Juan*).

MH370. Constrain by Inmarsat 7th-arc (00:19:29 UTC) and station geometry; evaluate H01W/H08S within tight windows; no signals were identified.



$$x_0 = \frac{(\hat{t}_2 - \hat{t}_1)c}{\left\{1 - \left[\frac{\pi c}{2h\hat{\Omega}_{t_2}}\right]^2\right\}^{-1/2} - \left\{1 - \left[\frac{\pi c}{2h\hat{\Omega}_{t_1}}\right]^2\right\}^{-1/2}};$$

$$t_0 = \hat{t}_j - \frac{x_0}{c} \left\{1 - \left[\frac{\pi c}{2h\hat{\Omega}_{t_j}}\right]^2\right\}^{-1/2}; \quad y_0 = \sqrt{(t_0 c)^2 - x_0^2},$$

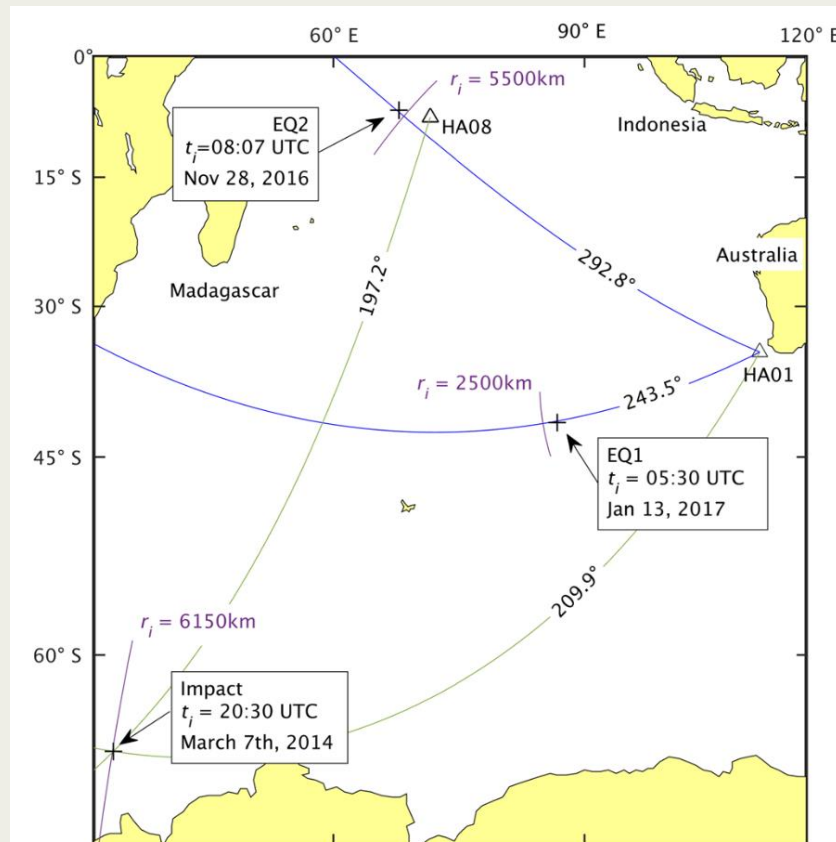


Figure 2. Great-circle orthodromic (or “shortest distance”) arcs (blue) from the hydrophone station HA01 indicate the bearing relative to the station of the incoming acoustic-gravity waves generated by distinct events. The distance r_i (purple arc) from the station is calculated using the inverse problem, and represents the highest probability (mode). The epicentre locations of the two earthquakes EQ1 and EQ2 and the triangulation from the station HA08 and HA01 for the 21:31:24 UTC event (green arcs) are also shown (+), together with the distance calculated with the inverse method. (Generated with Matlab R2016b Mapping Toolbox <https://uk.mathworks.com/products/mapping.html>. Public domain coastline data derived from Digital Chart of the World (DCW) available online at <http://gis-lab.info/qa/vmap0-eng.html>).